Challenges in using scanning lidars to estimate wind resources in complex terrain

Mann, Jakob; Menke, Robert; Vasiljevi, Nikola; Berg, Jacob; Troldborg, Niels

Published in:
Journal of Physics: Conference Series

Link to article, DOI:
10.1088/1742-6596/1037/7/072017

Publication date:
2018

Document Version
Publisher's PDF, also known as Version of record

Challenges in using scanning lidars to estimate wind resources in complex terrain

IOP Conf. Series: Journal of Physics: Conf. Series **1037** (2018) 072017 doi:10.1088/1742-6596/1037/7/072017

Challenges in using scanning lidars to estimate wind resources in complex terrain

Jakob Mann, Robert Menke, Nikola Vasiljević, Jacob Berg and Niels Troldborg

DTU Wind Energy, Technical University of Denmark, 4000 Roskilde, Denmark

E-mail: jmsq@dtu.dk

Abstract. Pairs of synchronously scanning Doppler lidars measure the average wind speed of flows crossing the parallel ridges at Perdigão, Portugal, with the ultimate purpose of wind resource estimation. The availability of the data from the lidars when they are running is quite low (50–70%). Furthermore, the instruments did only run less than half the time of the experimental period. These figures have to be improved in order for scanning lidars to be a viable option for wind resource estimation. The variations along the ridges are compared to neutral LES calculations making a good match at the upstream ridge but a significantly worse prediction at the downstream ridge. One reason could be an insufficient representation of the terrain. Another unknown is the influence of the atmospheric stability on the flow which is clearly seen by the scanning lidars.

1. Introduction

Imagine performing an experimental wind resource estimation campaign in complex terrain using long-range Doppler lidars being able to scan arbitrary trajectories. They could interrogate many potential wind turbine positions in the terrain rapidly collecting statistics used to pinpoint the most promising sites. Faster deployment, no need for building or environmental permits, and the possibility to cover many more points in the landscape are some of the advantages relative to meteorological mast deployments. Deployment of vertically profiling Doppler lidars also has some of these advantages but they still cover a limited number of positions in the landscape and they may suffer from biases in complex terrain due to the lack of homogeneity in the scanning cone [1]. The precision of the measurement of the 10-minute mean horizontal wind vector performed by several lidars focused at the same point is very high, of the order of one percent when compared to well-calibrated *in situ* measurements on a mast [2]. While the prospects of wind resource estimation by synchronized lidars are promising, many problems may arise. While the range for ordinary conically scanning lidars only needs to be a bit higher than the turbine height, i.e. a couple of hundred meters, the long-range scanning lidars to be used for wind resource estimation at multiple locations may need a range of several kilometers depending on the terrain. This demands a more powerful lidar and increases the risk of the beam being blocked by low-lying clouds or fog. Another risk is the reliability of the instruments. While ordinary conically scanning lidars have become quite robust, the longer range systems capable of doing almost arbitrary trajectories consume more energy, require more cooling, and are generally less robust.

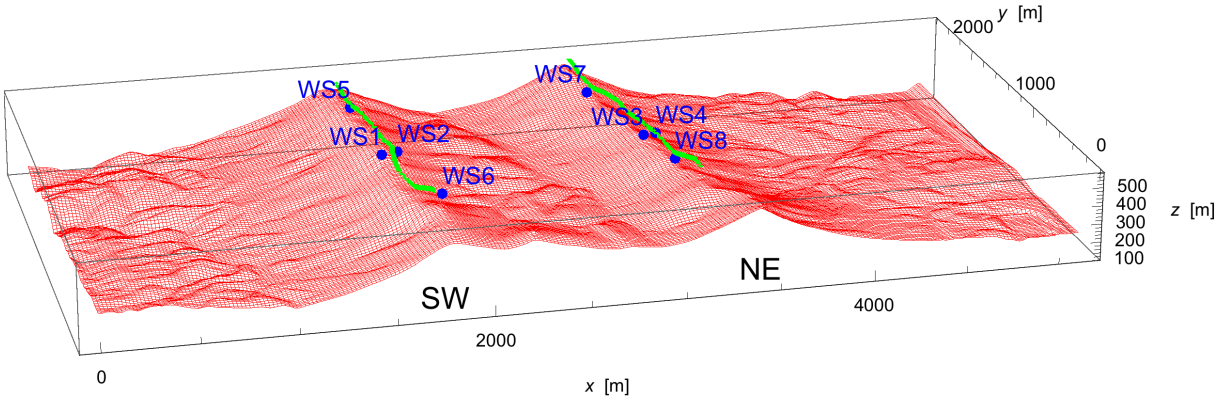

Figure 1. The computational domain showing the two parallel ridges, SW and NE, at Perdigão and the positions of the scanning lidars. WS5 and WS6 do synchronous scanning of the NE ridge along the green curve, while WS7 and WS8 scans the SW ridge approximately 80 m above the terrain. The terrain is derived from helicopter-borne lidar scanning.

This paper describes the deployment of lidars scanning the Perdigão ridges in Portugal. Perdigão is the largest of a series of field experiments in the on-going NEWA (New European Wind Atlas) Project [3]. The purpose of the experiments is to validate models for siting of wind turbines, in particular for wind resource estimation. We investigate the performance of the lidars and make a preliminary comparison with a large-eddy simulation (LES).

2. Experiment

The experiment had in total 20 scanning lidars but here we are focusing on pairs of lidars configured as dual-Doppler systems [4], doing scanning over the two ridges that constitute the Perdigão terrain. The lidars WS5 and WS6 were scanning 80 m above the opposing NE ridge while the instruments WS7 and WS8 were doing the same over the SW ridge. Each pair of scanners swept the opposing ridge along a 2 km long curve shown in green on figure 1. Each sweep lasted 45 s and the scans continued for a 10 min period which then was averaged.

The scanners WS1–4 did vertical scans along the line connecting the instruments.

From the pairs of scanners we get the two components of the wind vector in the plane spanned by the two beams which is slanted about 5° from horizontal.

The experiment started on March 27, 2017 and ended July 10, 2017 running for 105 days. The lidars ran in ridge scanning mode for 10 minutes every half hour doing other tasks for the other two 10-minute periods. 1981 10-minute periods were recorded corresponding to a total of 41 days (counting every period for half an hour). So the instruments were working in less than half of the period. Reasons for the ceased measurements ranged from software problems, overheating (many days had more than 40°C in the shade), and power outages.

3. Simulation

The simulation is carried out as LES using the Navier–Stokes flow solver EllipSys3D [5] with the sub grid scale model proposed by Deardorff [6]. Temperature effects are not included so the simulation assumes neutral conditions. The simulation is carried out in a terrain following curvilinear grid with dimensions $(L_x, L_y, L_z) = (5120\text{ m}, 2560\text{ m}, 3000\text{ m})$, where L_x , L_y and L_z is the domain length, width and height, respectively. The number of grid cells in each direction is $(N_x, N_y, N_z) = (256, 128, 128)$. Figure 1 shows the horizontal extent of the computational domain in a three-dimensional perspective together with the position of all scanning lidars operated by DTU and the tracks of the "ridge scans". For this preliminary computation, the

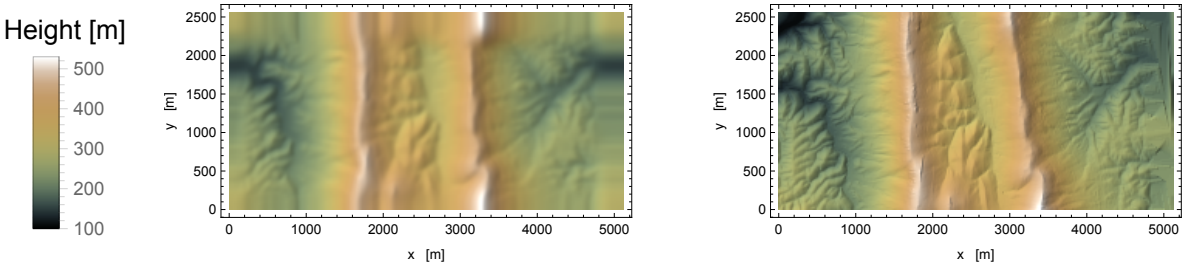

Figure 2. Original surface (right) and surface used in the cfd (left).

Coriolis force was ignored. Also, a uniform roughness is assumed with $z_0 = 0.5$ m and the flow is driven with a constant pressure gradient of $\partial p/\partial x = \rho u_*^2/L_z$, where $u_* = 0.6$ m/s is the friction velocity, i.e. in the direction from the SW towards the NE roughly perpendicular to the ridges. Periodic boundary conditions are applied in both the x and y directions in the following way. The right and the top edge heights are copied to the left and the bottom boundary of the map. A horizontal gradient is enforced at all four edges and the changes to the topography is propagated 30 grid cells away from the edges. Each grid cell has horizontal dimensions of $\Delta x = \Delta y = 20$ m. The effect of the edge treatment can be seen on the left plot of figure 2. In addition to this, a Gaussian Fourier filtering on the terrain has been performed in which the Fourier transform of the terrain height $\hat{h}(k_x, k_y)$ is multiplied by $\exp(-\frac{1}{2}(k_x^2\Delta x^2 + k_y^2\Delta y^2))$ and then Fourier transformed back. The reason for doing this is to speed up the convergence of the cfd solvers but the exact consequences of this smoothing remains to be investigated. The original surface (right plot in figure 2) is derived from a helicopter-borne back-scatter lidar scan with a density of 45 points per square meter. From these the ground elevation is found on a 2 by 2 meter grid which is then sampled at every 20 m. The canopy height and density is also derived but the impact of this is also left for future investigations. The original map appears sharper than the one used in the cfd and the rightmost ridge appears to have a slightly different orientation due to the imposed periodicity.

The symmetry condition is assumed on the top boundary and a log law is assumed at the ground. Because of periodicity there is no inflow condition.

For a detailed discussion of the simulation and a snapshot of the flow, see paper by Berg *et al* in these proceedings.

4. Results and discussion

Two examples of 10-minute average wind vectors are shown in figure 3. The base of the wind vectors on each plot are the scan positions seen from above corresponding to the green curves on figure 1. These are rare examples where the instruments were capable of measuring at every point on both ridges simultaneously.

In figure 4 the availability of data is shown. The fraction shown is the percentage of the 1982 measurement periods where a 10-minute mean is obtained. Often only one pair of scanners was working and the instruments scanning the NE ridge was working approximately 70% of the time. The lidars scanning the SW were not working that well, barely reaching 50% availability. When demanding both pairs of lidars working simultaneously the availability is even worse, reaching around 30%. The dip in availability of the NE ridge data around position 58 is due to interference between the laser beam and guyed cable of a 100 m mast while the dip around position 47 on the SW ridge data is due to interference with a wind turbine at that position. Irregularities at these positions can also be seen in the example vector plots in figure 3. In general, it can be seen that the availability decreases towards the end of the ridge paths. At

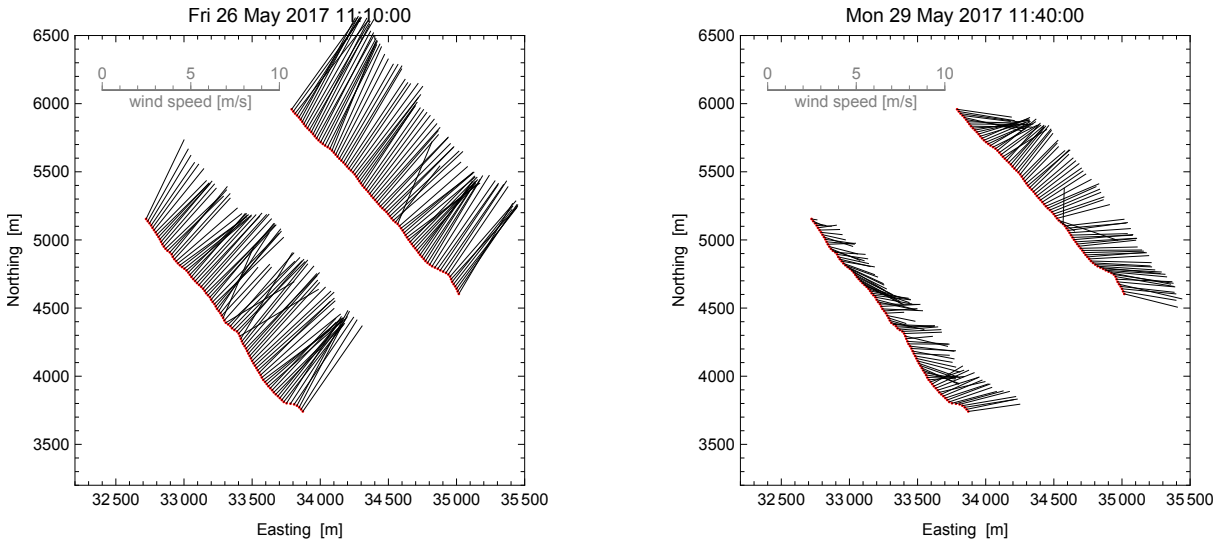

Figure 3. Example 10-minute average two-dimensional wind vectors.

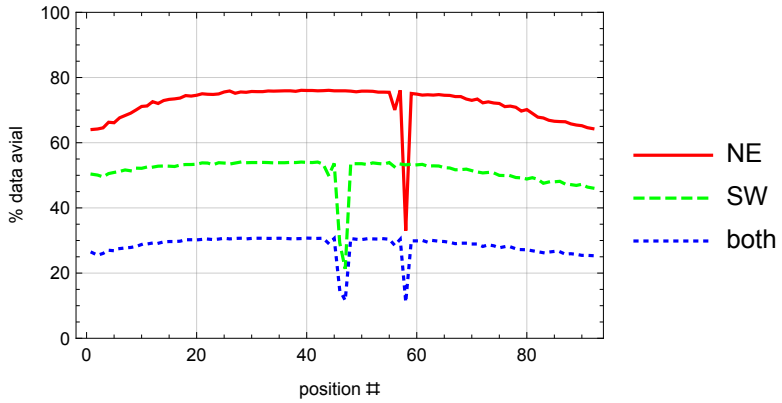

Figure 4. Availability of data at the 92 positions at each ridge. Positions are counted from NW.

these ends, one of the instruments will have a long range and we believe that is the cause of this decrease.

An overview of data recorded simultaneously at the two ridges is shown in figure 5. In order to suppress outliers we show the median of all the 10-minute mean wind vectors on each ridge so the wind speeds and the directions in these plots are derived from from these median vectors. The directions are using the geographical convention with 0° corresponding to winds from the north and with wind direction increasing clockwise. It can be seen that when the wind is from the NE (points in yellowish or orange colors) there is a tendency for the wind on the downwind SW ridge to be *larger*. There also seems to be a slight turning of the wind towards east on the SW ridge relative to the NE ridge for these wind directions. For winds from the SW the wind speed and direction changes seem to be smaller.

From the two components of the 10 min mean wind speed we calculate the length U of this two-dimensional vector as a function of distance along the green curve shown in figure 1. The distance is measured from the NW end of the curves, that is, starting from WS5 or WS7, see figure 1. Only cases where the median wind speed and direction on any ridge is with $\pm 20°$ of the

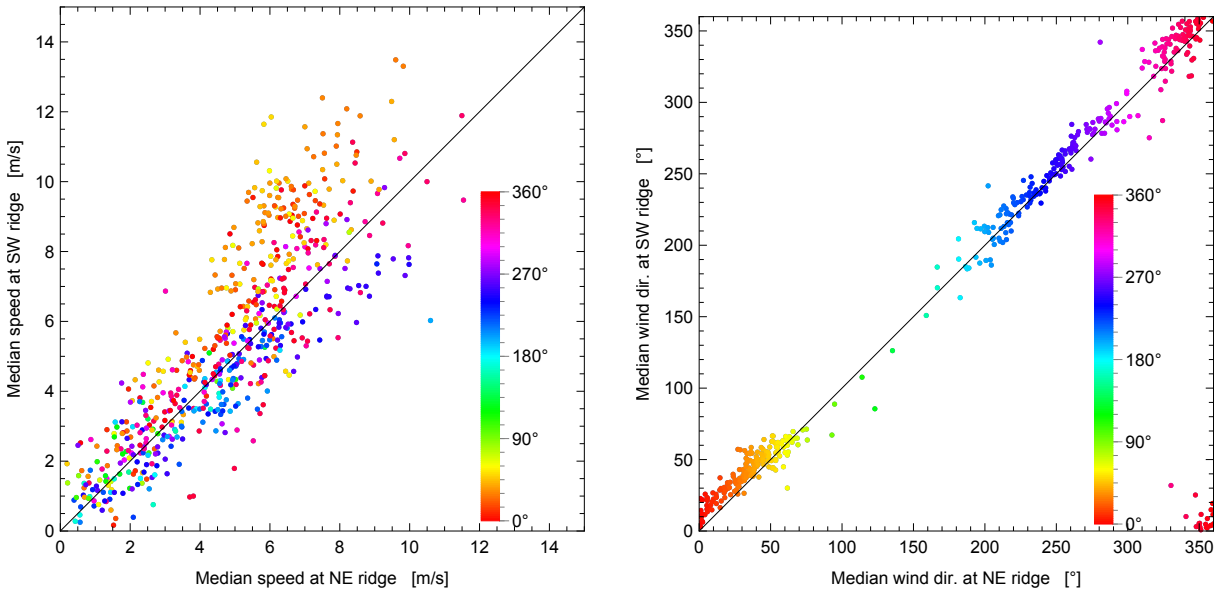

Figure 5. Overview of data obtained simultaneously on both ridges. On the left plot is the median wind speed (in m/s) at each ridge. To the right is the corresponding wind directions (in °) but only when the wind speed (at the NE ridge) is larger than 3 m/s.

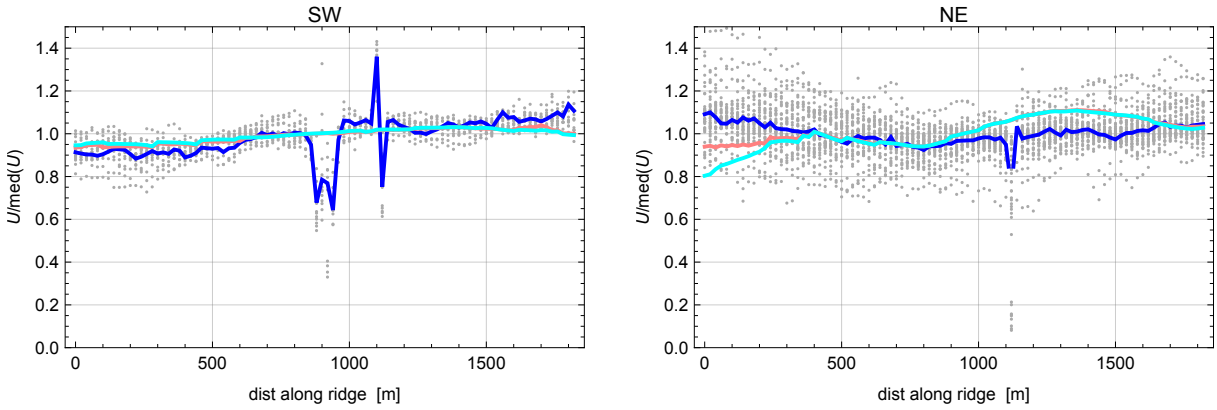

Figure 6. Measurements of the median normalized 10 min. wind speed for flow from the SW towards the NE (gray points) on both ridges. The median is shown in blue. The simulations normalized in the same way are shown in cyan and pink (partly hidden), the first being sampled 80 m above the terrain, the second 80 m above the smoothed terrain.

direction used in the computation and larger than 7 m/s to try to ensure neutral atmospheric stability are plotted All wind speed are divided by the median of wind speed along the ridge from each 10 min period to emphasize the variations along the ridge and not the actual wind speed or the wind speed ratio between the two ridges.

All normalized 10 min averages are plotted in figure 6 and the median of those at each position is shown as a blue curve. The kinks occurring near 1120 m on the NE ridge and at 900 and 1100 m at the SW ridge are due to interference of the laser beams with either guyed cables on a mast or a wind turbine on the SW ridge, as discussed previously in connection with figure 4. In addition to that, the rapid fluctuations around 1100 m on the SW ridge is probably due to another 100 m mast located at this position.

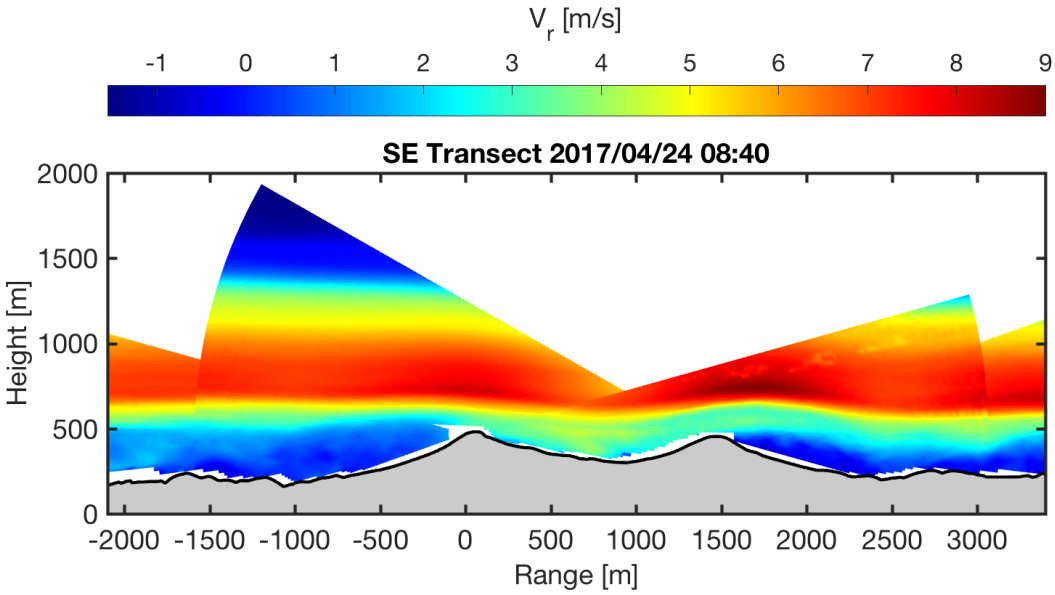

Figure 7. Cross-section of stably stratified flow over Perdigão. The colors are the line-of sight velocities V_r with positive values corresponding to flow from left to right. The SW ridge is at range equal to 0 m and the NE ridge is at 1500 m.

It can be seen from figure 6 that the variations of the wind speed are captured well by the model on the upwind SW ridge but not very well on the downwind NE ridge. The large discrepancies for distances along the ridge of less than 400 m can be attributed to the enforced periodicity of the terrain and can be disregarded. The reasons for the discrepancy at distances along the ridge larger than 400 m are many:

- The terrain is represented by a uniform roughness in the computations while the hills are covered by stands of eucalyptus and pine of very different heights.
- Details in the terrain not represented in the computation may affect the flow [7].
- The atmospheric stability is assumed to be neutral and the Coriolis force is ignored.
- The computational domain is probably too narrow.

Windscanners WS1–4 show how much stability affects the flow, even at relatively high winds. In figure 7, a morning flow that appears to be stably stratified shows wavy structures over the ridges and strong stagnation upstream of the SW ridge. Such effects are not taken into account by the present flow model and we will briefly investigate the biases caused by this assumption. There is also a stagnant recirculation zone behind the downstream NE ridge. The $U > 7$ m/s criterion for neutral startification is now investigated in more detail by calculating the Richardson number based on data from a 100 m mast located on the SW ridge. The Richardson is defined as

$$Ri = \frac{g/T\partial\theta_v/\partial z}{(\partial U/\partial z)^2 + (\partial V/\partial z)^2} \tag{1}$$

where g is the acceleration due to gravity, T the temperature, U and V the two horizontal components of the mean wind vector, and θ_v the virtual potential temperature. It is not straight

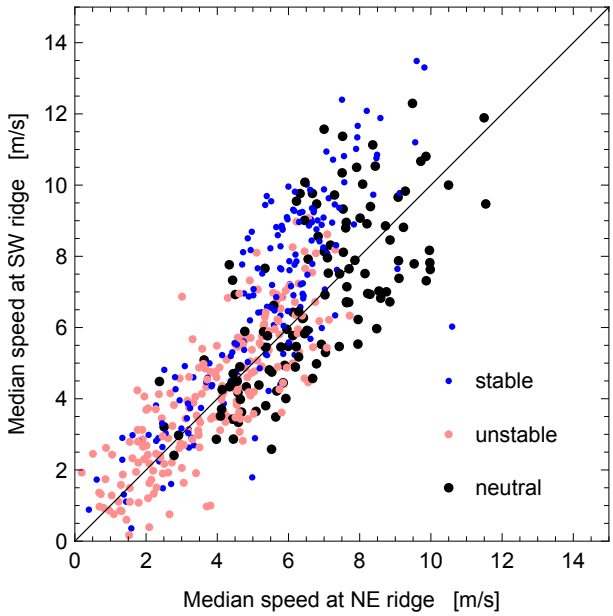

Figure 8. Median wind speeds at the two ridges as in figure 5 left but now colored according to stability.

forward to use this definition in complex terrain. Even under near-neutral conditions the gradient of the mean wind speed can become zero above the ridge due to the speed up implying an infinite Ri. Therefore we choose to approximate the velocity gradients by the finite difference of the wind speed at 100 m and that at 0 m (which is 0 m/s). The temperature gradients are the mast measured finite differences using measurements at 10 m and 100 m. The Richardson numbers are calculated using 30 minutes of data that includes the 10-minute ridge scans.

The median wind speeds at the two ridges are plotted in figure 8 again versus each other as in figure 5 (left) sorted according to stability. We define stable as $Ri > 0$, neutral $-0.18 < Ri < 0$ and unstable $Ri < -0.18$. This division is based on comparison with diurnal cycle.

We see that most unstable runs have $U < 7$ m/s but that many stable runs have higher wind speeds. There seems to be a tendency that the winds on the SW ridge are relatively larger for stable conditions compared to neutral conditions.

5. Conclusion

We are a long way from being able to use synchronized long-range, scanning lidars for routine wind resource estimation in complex terrain. While we have no reason to question the measured wind speeds and directions when the beams are not disturbed by wind turbines or masts, the availability of the systems and the data is so far a major shortcoming. Software, cooling systems, etc., have to be improved significantly. Availability could also be improved by sophisticated lidar data filtering as suggested in [8].

Comparison with LES show some encouragement but it is almost certain that the heterogeneity of the terrain surface and the atmospheric stratification which have so far been ignored in the computations will have a significant effect on the results as tentatively seen by the analysis of stability data.

References

[1] Bingöl F, Mann J and Foussekis D 2009 *Meteorologische Zeitschrift* **18** 189–195

[2] Pauscher L, Vasiljevic N, Callies D, Lea G, Mann J, Klaas T, Hieronimus J, Gottschall J, Schwesig A, Kühn M *et al.* 2016 *Remote Sensing* **8** 782
[3] Mann J, Angelou N, Arnqvist J, Callies D, Cantero E, Arroyo R C, Courtney M, Cuxart J, Dellwik E, Gottschall J *et al.* 2017 *Phil. Trans. R. Soc. A* **375** 20160101
[4] Vasiljević N, Lea G, Courtney M, Cariou J P, Mann J and Mikkelsen T 2016 *Remote Sensing* **8** 896
[5] Sørensen N N 1995 General purpose flow solver applied to flow over hills PhD thesis Risø–R–864(EN) Risø National Laboratory
[6] Deardorff J W 1980 *Boundary-Layer Meteorology* **18** 495–527
[7] Lange J, Mann J, Berg J, Parvu D, Kilpatrick R, Costache A, Chowdhury J, Siddiqui K and Hangan H 2017 *Environmental Research Letters* **12** 094020
[8] Beck H and Kühn M 2017 *Remote Sens-Basel* **9** 561